

Activated peripheral blood mononuclear cell mediators trigger astrocyte reactivity



Bruna Bellaver^a, Andréia S. Rocha^a, Débora G. Souza^a, Douglas T. Leffa^b, Marco Antônio De Bastiani^a, Guilherme Schu^a, Pâmela C. Lukasewicz Ferreira^c, Gianina T. Venturin^d, Samuel Greggio^d, Camila T. Ribeiro^a, Jaderson C. da Costa^d, José Cláudio Fonseca Moreira^{a,e}, Daniel P. Gelain^{a,e}, Iraci Lucena da S. Torres^{b,f,h}, Fábio Klamt^{a,g}, Eduardo R. Zimmer^{a,f,h,*}

^a Graduate Program in Biological Sciences: Biochemistry, Universidade Federal do Rio Grande do Sul, Porto Alegre, Brazil

^b Graduate Program in Medicine: Medical Sciences, Universidade Federal do Rio Grande do Sul, Porto Alegre, Brazil

^c Graduate Program in Pharmaceutical Science, Universidade Federal do Rio Grande do Sul, Porto Alegre, Brazil

^d Preclinical Imaging Center, Brain Institute (BraIns) of Rio Grande do Sul, Porto Alegre, Brazil

^e Department of Biochemistry, Universidade Federal do Rio Grande do Sul, Porto Alegre, Brazil

^f Graduate Program in Biological Sciences: Pharmacology and Therapeutics, Universidade Federal do Rio Grande do Sul, Porto Alegre, Brazil

^g Laboratory of Cellular Biochemistry, Instituto de Ciências Básicas da Saúde, Universidade Federal do Rio Grande do Sul, Porto Alegre, Brazil

^h Department of Pharmacology, Universidade Federal do Rio Grande do Sul, Porto Alegre, Brazil

ARTICLE INFO

Keywords:

Astrocyte
Glucose
Glutamate
Energy metabolism
PBMC
Sepsis

ABSTRACT

Sepsis is characterized by a severe and disseminated inflammation. In the central nervous system, sepsis promotes synaptic dysfunction and permanent cognitive impairment. Besides sepsis-induced neuronal dysfunction, glial cell response has been gaining considerable attention with microglial activation as a key player. By contrast, astrocytes' role during acute sepsis is still underexplored. Astrocytes are specialized immunocompetent cells involved in brain surveillance. In this context, the potential communication between the peripheral immune system and astrocytes during acute sepsis still remains unclear. We hypothesized that peripheral blood mononuclear cell (PBMC) mediators are able to affect the brain during an episode of acute sepsis. With this in mind, we first performed a data-driven transcriptome analysis of blood from septic patients to identify common features among independent clinical studies. Our findings evidenced pronounced impairment in energy-related signaling pathways in the blood of septic patients. Since astrocytes are key for brain energy homeostasis, we decided to investigate the communication between PBMC mediators and astrocytes in a rat model of acute sepsis, induced by cecal ligation and perforation (CLP). In the CLP animals, we identified widespread *in vivo* brain glucose hypometabolism. *Ex vivo* analyses demonstrated astrocyte reactivity along with reduced glutamate uptake capacity during sepsis. Also, by exposing cultured astrocytes to mediators released by PBMCs from CLP animals, we reproduced the energetic failure observed *in vivo*. Finally, by pharmacologically inhibiting phosphoinositide 3-kinase (PI3K), a central metabolic pathway downregulated in the blood of septic patients and reduced in the CLP rat brain, we mimicked the PBMC mediators effect on glutamate uptake but not on glucose metabolism. These results suggest that PBMC mediators are capable of directly mediating astrocyte reactivity and contribute to the brain energetic failure observed in acute sepsis. Moreover, the evidence of PI3K participation in this process indicates a potential target for therapeutic modulation.

1. Introduction

Sepsis is characterized by a severe and disseminated systemic

inflammation as a result of a microorganism invasion in the bloodstream. In this inflammatory scenario, the activation of the peripheral immune system also affects brain function. Reports have demonstrated

* Corresponding author at: Department of Pharmacology, Universidade Federal do Rio Grande do Sul (UFRGS), 2500 Ramiro Barcelos Street, 90035-003 Porto Alegre, RS, Brazil.

E-mail address: eduardo.zimmer@ufrgs.br (E.R. Zimmer).

URL: <http://www.zimmer-lab.org> (E.R. Zimmer).

<https://doi.org/10.1016/j.bbi.2019.05.041>

Received 9 January 2019; Received in revised form 28 May 2019; Accepted 30 May 2019

Available online 05 June 2019

0889-1591/ © 2019 Elsevier Inc. All rights reserved.

that sepsis impairs the brain even earlier than other organs, which increases morbidity and mortality rates in this condition (Michels et al., 2015; Young, 2010; Ziája, 2013). Moreover, long-term brain dysfunction is commonly observed in sepsis-survivors (Iwashyna et al., 2010). However, key systemic features triggering brain impairment during acute sepsis are still elusive. In this context, it has been suggested that glial cells have a significant role in mediating the crosstalk between systemic immune signals and the central nervous system (CNS) (Bellaver et al., 2017; Michels et al., 2015; Richards et al., 2015).

In the acute phase of sepsis, inflammation is coordinated by the innate immune system. In this scenario, the activation of peripheral blood mononuclear cells (PBMCs), is thought to play an important role in orchestrating this immune response as PBMCs actively change their transcriptomic and secretory profile (Godini and Fallahi, 2018; Ransohoff et al., 2015; Tang et al., 2009), being able to release mediators to the affected sites, which include the brain (Ransohoff et al., 2015). Additionally, an elevated rate of PBMC infiltration into the CNS under inflammatory conditions was previously demonstrated (Kyrkanides et al., 2008). Based on this, it is very likely that infiltrated PBMCs, or their mediators, are capable of activating brain immune cells, such as microglia and astrocytes. In this way, recent evidence suggests a potential microglial-independent direct activation of astrocytes by PBMCs (Hornig et al., 2017; Richards et al., 2015). When activated, astrocytes overexpress the astrocytic glial fibrillary acidic protein (GFAP) and undergo morphological changes, becoming reactive (Sofroniew, 2009).

Astrocytes are important regulators of brain homeostasis. They directly modulate glutamatergic neurotransmission by taking up glutamate from the synaptic cleft through highly efficient glutamate transporters (Souza et al., 2019). Astroglial glutamate transport is suggested as a main signaling trigger for glucose uptake in astrocytes (Pellerin and Magistretti, 2012). In fact, glutamate transport activation via glutamate transporter-1 (GLT-1) increases glucose metabolism *in vivo* as indexed by [¹⁸F]fluorodeoxyglucose ([¹⁸F]FDG) positron emission micro-tomography (microPET) (Zimmer et al., 2017). Therefore, it suggests that [¹⁸F]FDG signal also reflects astrocyte metabolism, reinforcing a central participation of these glial cells in brain energy metabolism (Nortley and Attwell, 2017; Zimmer et al., 2017).

Based on this, this study is intended to evaluate the crosstalk between peripheral mediators and astrocytes during the acute phase of sepsis. We hypothesized that peripheral immune signals sent by PBMCs are capable of triggering astrocyte reactivity and, consequently, impacting brain energetic metabolism.

2. Material and methods

2.1. Microarray data acquisition, differential gene expression (DEG) and enrichment analysis

Human blood expression datasets from 250 healthy subjects and 277 sepsis patients were obtained from the Gene Expression Omnibus repository (GEO) (<http://www.ncbi.nlm.nih.gov/geo/>). Table 1 summarizes the data from the 10 selected GEO datasets used in this study. All transcriptomic analyses were implemented in an R statistical environment. Differential expression analysis was computed for each dataset independently, using the LIMMA package (Ritchie et al., 2015), and considering FDR-adjusted p-value < 0.05 as DEG criteria. Only genes significantly expressed in more than 7 datasets were included in further analyses. Hierarchical clustering of DEGs median logFC was constructed using Euclidean distance and Wards hierarchical agglomerative clustering criterion (Murtagh and Legendre, 2014). Finally, functional enrichment analyses of gene ontology (GO) biological processes and KEGG pathways were computed using the cluster Profiler and GOpilot packages (Yu et al., 2012).

2.2. Chemicals

DNase and LY 294002 were obtained from Sigma-Aldrich (St. Louis, MO, USA). TRIzol Reagent, Dulbecco's modified Eagle's medium/F12 (DMEM/F12), and other materials for cell culture were purchased from Gibco/Invitrogen/Thermo (Carlsbad, CA, USA). Polyclonal anti-GFAP was purchased from Dako (Carpinteria, CA, USA). Monoclonal β -actin and 4,6-diamino-2-phenylindole (DAPI) were purchased from Millipore (Billerica, MA, USA). Alexa Fluor® 488 (Amax = 493; Emax = 519) conjugated AffiniPure antibodies were purchased from Jackson ImmunoResearch (West Grove, PA, USA). L-[³H]-glutamate, 2-Deoxy-D-[1,2-³H]glucose ([³H]2DG), nitrocellulose membrane and ECL kit were from Amersham. All other chemicals were purchased from common commercial suppliers.

2.3. Animals

Adult male Wistar rats (90 days old) were divided into two groups: sham ($n = 13$; bodyweight = 375 ± 36 g) and CLP ($n = 14$; bodyweight = 390 ± 34 g). Newborn rats (1–2 days old) were used for experimental primary astrocyte cultures ($n = 40$). All animals were obtained from our breeding colony (Department of Biochemistry, UFRGS, Porto Alegre, Brazil), maintained in a controlled environment (12 h light/12 h dark cycle; 22 ± 1 °C; ad libitum access to food and water). All animal experiments were performed in accordance with the National Institute of Health (NIH) Guide for the Care and Use of Laboratory Animals and the Brazilian Society for Neuroscience and Behavior recommendations for animal care. The experimental protocols were approved by the Federal University of Rio Grande do Sul Animal Care and Use Committee.

2.4. Cecal ligation and perforation (CLP) in Wistar rats

For induction of systemic inflammation, male Wistar rats were subjected to CLP as previously described (Petronilho et al., 2012). Rats were anesthetized with a mixture of ketamine and xylazine, given intraperitoneally. A 3 cm midline laparotomy was performed to allow exposure of the cecum with the adjoining intestine. The cecum was tightly ligated with a 3.0 nylon suture at its base, below the ileocecal valve, maintaining bowel flow continuity, and was perforated once with a 14-gauge needle. The cecum was then gently squeezed to extrude a small amount of fecal material from the perforation site and then returned to the peritoneal cavity. The laparotomy was closed with 4.0 nylon sutures and the rats were returned to their cages. Animals were resuscitated with normal saline (50 mL/kg subcutaneously) immediately and 12 h after CLP. In the sham-operated group, rats were submitted to all surgical procedures but the cecum was neither ligated nor perforated. In absence of antibiotic therapy, the mortality rate in this model was 100% after 72 h. All *in vivo* and *in vitro* analyses were performed after 24 h. of CLP when there was no mortality but the animals were lethargic, presenting piloerection, diarrhea, huddling along with an increase in BBB permeability (Supplementary Fig. 1). After surgery, no differences in food intake between groups were identified.

2.5. Micro-PET brain scan

Twenty-four hours after surgical induction of sepsis, the animals from each group (sham $n = 13$ and CLP $n = 14$) were individually anesthetized using a mixture of isoflurane and medical oxygen (3–4% induction dose), and injected with 0.4 mL [¹⁸F]FDG (sham = 38.05 ± 1.06 MBq and CLP = 37.56 ± 1.08 MBq) in the tail vein, after overnight fasting. Then, each rat was returned to its home cage for a 40 min period of conscious (awake) *in vivo* metabolism of [¹⁸F]FDG. After the uptake period, each rat was placed in a head-first prone position and scanned with the Triumph™ micro-PET [LabPET-4, TriFoil Imaging, Northridge, CA, USA, (for LabPET-4 technical

Table 1
Gene expression microarray data used for transcriptome analysis.

GEO ID	Description	Sample (n)	Reference
GSE95233	Gene expression data of whole blood collected from patients at day 1 of sepsis and from healthy subjects	Whole blood from septic patients (n = 51) Whole blood from healthy subjects (n = 22)	Venet et al. (2017)
GSE49757	Gene expression data of polymorphonuclear neutrophils collected from septic patients in the first admission at hospital and from healthy subjects	Polymorphonuclear neutrophils from septic patients (n = 35) Polymorphonuclear neutrophils from healthy subjects (n = 19)	Not published
GSE67652	Gene expression data of polymorphonuclear neutrophils collected from septic patients and from healthy subjects with paired age	Polymorphonuclear neutrophils from septic patients (n = 6) Polymorphonuclear neutrophils from healthy subjects (n = 6)	da Silva et al. (2015)
GSE57065	Gene expression data of whole blood collected from patients 24 h after septic shock and from healthy subjects	Whole blood from septic patients (n = 28) Whole blood from healthy subjects (n = 25)	Cazalis et al. (2014)
GSE54514	Gene expression data of whole blood collected from patients at day 1 of sepsis and from healthy subjects	Whole blood from septic patients (n = 26) Whole blood from healthy subjects (n = 18)	Parnell et al. (2013)
GSE32707	Gene expression data of whole blood collected from septic patients in the first admission at hospital and from healthy subjects	Whole blood from septic patients (n = 34) Whole blood from healthy subjects (n = 38)	Dolinay et al. (2012)
GSE28750	Gene expression data of polymorphonuclear neutrophils collected from septic patients in the first admission at hospital and from healthy subjects	Polymorphonuclear neutrophils from septic patients (n = 27) Polymorphonuclear neutrophils from healthy subjects (n = 20)	Sutherland et al. (2011)
GSE13015	Gene expression data of whole blood collected from septic patients and healthy subjects	Whole blood from septic patients (n = 31) Whole blood from healthy subjects (n = 29)	Pankla et al. (2009)
GSE69063	Gene expression data of whole blood collected from septic patients and healthy subjects	Whole blood from septic patients (n = 33) Whole blood from healthy subjects (n = 57)	Not published
GSE46955	Gene expression data of monocytes collected from septic patients in the first admission at hospital and from healthy subjects	Monocytes from septic patients (n = 6) Monocytes from healthy subjects (n = 16)	Shalova et al. (2015)

information see Bergeron et al., 2014)] under inhalational anesthesia (2–3% maintenance dose). Throughout these procedures, the animals were kept on a pad heated at 37 °C. For radiotracer readings, 10 min list mode static acquisitions were acquired with the field of view (FOV; 3.75 cm) centered on each rat's head (Zanirati et al., 2018). All data were reconstructed using the maximum likelihood estimation method (MLEM-3D) algorithm with 20 iterations. Each micro-PET image was reconstructed with a voxel size of 0.2 × 0.2 × 0.2 mm and spatially normalized into an [¹⁸F]FDG template using brain normalization in PMOD v3.8 and the Fuse It Tool (PFUSEIT) (PMOD Technologies, Zurich, Switzerland). An MRI rat brain volume of interest (VOI) template was used to overlay the normalized images previously coregistered to the micro-PET image database. Activity values were normalized for the injected dose and the animal bodyweight, and were therefore expressed in standard uptake values (SUVs). Mean SUVs of 14 brain regions were extracted using a predefined VOI template. For analysis at the voxel level, MINC tools (www.bic.mni.mcgill.ca/ServicesSoftware) were used for image processing and analysis.

2.6. Metabolic networks

Metabolic brain networks of groups were constructed by computing Pearson correlation coefficients based on 10,000 bootstrap samples. Graph theoretical measures such as density, global efficiency, small-world, assortativity coefficient, average degree and average clustering coefficient were calculated for each of the bootstrap samples. Networks were corrected for multiple comparisons using false discovery rate $P < 0.005$ (Rubinov and Sporns, 2010).

2.7. Hippocampal primary astrocyte cultures and maintenance

Twenty-four hours after CLP induction, animals from both groups had their cerebral hippocampi aseptically dissected and their meninges removed. The astrocyte cultures were performed as previously described (Bellaver et al., 2017; Bellaver et al., 2016b). During the dissection, cerebral tissue was kept in HBSS (Hank's Balanced Salt Solution) containing 0.05% trypsin and 0.003% DNase at 37 °C for 8 min. The tissue was then mechanically dissociated for 7 min using a Pasteur

pipette and centrifuged at 100 xg for 5 min. The pellet was resuspended in a solution of HBSS containing only 0.003% DNase and again gently mechanically dissociated for 5 min with a Pasteur pipette and left for decantation for 20 min. The supernatant was collected and centrifuged for 7 min. (100 xg). The cells from the supernatant were resuspended in DMEM/F12 [10% fetal bovine serum (FBS), 15 mM HEPES, 14.3 mM NaHCO₃, 0.04% gentamicin and 1% Fungizone®], plated in 6- or 24-well plates pre-coated with poly-L-lysine and cultured at 37 °C in an incubator with 5% CO₂. The cells were seeded at 3–5 × 10⁵ cells/cm². The same protocol was applied to cultivate astrocytes from newborn (naive) animals. The first medium exchange occurred 24 h. after obtaining cultures. During the 1st week, the change occurred once every two days and from the 2nd week on, the change occurred once every four days. From the 3rd week on, hippocampal astrocytes received the culture medium supplemented with 20% FBS. Around the 4th week, the cells reached confluence, and biochemical and molecular analyses were performed by researchers blinded for group allocation.

2.8. 2-Deoxy-D-[1,2-³H]glucose ([³H]2DG) uptake

After cells reached confluence, glucose was assessed as previously described (Souza et al., 2013). Briefly, cells were rinsed once with HBSS and incubated with DMEM/F12 containing only 1 mCi/ml [³H]2DG (basal) or 1 mCi/ml [³H]2DG + 100 μM glutamate (stimulated) for 20 min at 37 °C. After incubation, astrocytes were rinsed with HBSS and lysed overnight with NaOH 0.3M. Incorporated radioactivity was measured in a scintillation counter. Cytochalasin B (10 mM) was used as a specific glucose transporter inhibitor. Glucose uptake was determined by subtracting uptake with cytochalasin B from total uptake.

2.9. Glutamate uptake

After the cells reached confluence, glutamate uptake was determined as previously described (Bellaver et al., 2016a). Briefly, astrocyte cultures were incubated at 37 °C in HBSS containing the following components (in mM): 137 NaCl, 5.36 KCl, 1.26 CaCl₂, 0.41 MgSO₄, 0.49 MgCl₂, 0.63 Na₂HPO₄, 0.44 KH₂PO₄, 4.17 NaHCO₃, and 5.6 glucose, adjusted to pH 7.4. The assay was started by the addition of

100 μ M L-glutamate and 0.33 μ Ci/ml L-[2,3- 3 H] glutamate. The incubation was stopped after 7 min by removing the medium and rinsing the wells twice with ice-cold HBSS. The cells were then lysed in a solution containing 0.5 M NaOH. Incorporated radioactivity was measured in a scintillation counter. Sodium-independent uptake was determined using methyl-D-glucamine instead of sodium chloride. Sodium-dependent glutamate uptake was obtained by subtracting the sodium-independent uptake from the total uptake.

2.10. High-performance liquid chromatography (HPLC) procedure

The assay was performed to measure glutamate levels in the cerebrospinal fluid (CSF) of animals 24 h. after CLP or sham surgery. Briefly, the CSF was filtered (0.22 μ m pore), samples were derivatized with o-phthalaldehyde and separation was carried out with a reverse phase column (Supelcosil LC-18, 250 mm \times 4.6 mm, Supelco) in a Shimadzu Class-VP chromatography system. The mobile phase flowed at a rate of 1.4 mL/min. and column temperature was 24 $^{\circ}$ C. Buffer composition was A: 0.04 mol/L sodium dihydrogen phosphate monohydrate buffer, pH 5.5, containing 20% of methanol; B: 0.01 mol/L sodium dihydrogen phosphate monohydrate buffer, pH 5.5, containing 80% of methanol. The gradient profile was modified according to the content of buffer B in the mobile phase: 0% for 0.00 min, 100% for 55 min, 0% for 55–60.00 min. Absorbance was read at 360 nm and 455 nm, excitation and emission respectively, with a Shimadzu fluorescence detector.

2.11. RNA extraction and quantitative RT-PCR

Total RNA was isolated from primary astrocyte cultures obtained from sham/CLP animals using TRIzol Reagent (Invitrogen, Carlsbad, CA). The concentration and purity of the RNA were determined spectrophotometrically at a ratio of 260/280. Then, 1 μ g of total RNA was reverse transcribed using Applied Biosystems™ High-Capacity cDNA Reverse Transcription Kit (Applied Biosystems, Foster City, CA) in a 20 μ L reaction, according to manufacturer's instructions. The mRNAs of GLT-1 and glutamate-aspartate transporter (GLAST) were quantified using a TaqMan real-time RT-PCR system with inventory primers and probes purchased from Applied Biosystems (Foster City, CA). Quantitative RT-PCR was performed in duplicate using the Applied Biosystems 7500 Fast system. No-template and no-reverse transcriptase controls were included in each assay, and these produced no detectable signal during the 40 cycles of amplification. Target mRNA levels were normalized using β -actin as a housekeeper gene. The results were expressed as fold of change of sham group using the $2^{-\Delta\Delta C_t}$ method (Livak and Schmittgen, 2001).

2.12. Western blot analysis

Hippocampal astrocytes from sham/CLP animals or PBMC CM treated animals were solubilized in lysis solution containing 4% SDS, 2-mM EDTA and 50-mM Tris-HCl (pH 6.8). Samples were separated by SDS/PAGE (15 mg protein per sample), and transferred to nitrocellulose membranes, which were then incubated overnight (4 $^{\circ}$ C) with one of the following antibodies: anti-GFAP (1:1000), anti-GLT-1 (1:1000), anti phospho-phosphoinositide 3-kinase (PI3K) p85 (Tyr458)/p55 (Tyr199) (1:1000) or anti- β -actin (1:5000). β -actin was used as a loading control. Then, the membranes were incubated with a peroxidase-conjugated anti-rabbit or anti-mouse immunoglobulin (IgG) (1:7000) for 1 h. Chemiluminescence signals were detected in an Image Quant LAS4010 system (GE Healthcare) using an ECL kit (Souza et al., 2016b).

2.13. Immunofluorescence analysis

Immunofluorescence was performed as described previously by our group (Souza et al., 2016a). Cell cultures were fixed with 4%

paraformaldehyde for 20 min and permeabilized with 0.1% Triton X-100 in PBS for 5 min at room temperature. After blocking overnight with 4% albumin, the cells were incubated overnight with anti-GFAP (1:400) at 4 $^{\circ}$ C. Then, an incubation with a secondary antibody conjugated with Alexa Fluor® 488 for 1 h at room temperature was performed. For all the immunostaining-negative control reactions, the primary antibody was omitted. No reactivity was observed when the primary antibody was excluded. For actin-labeling analyses, the cells were incubated with 10 mg/ml rhodamine-labeled phalloidin in PBS for 45 min. Cell nuclei were stained with 0.2 mg/ml of 4',6'-diamino-2-phenylindole (DAPI) for 10 min. Astrocyte immunofluorescence was analyzed and photographed with a Nikon microscope and a TE-FM Epi-Fluorescence accessory.

2.14. Multiplex assays

Cell-free supernatants of cultivated PBMCs and serum of sham and CLP rats were assayed for the presence of the following inflammatory mediators: interleukin (IL)-1 α , IL-1 β , granulocyte-macrophage colony-stimulating factor (GM-CSF), granulocyte colony-stimulating factor (G-CSF), interferon gamma (INF- γ), IL-2, IL-4, IL-5, IL-6, IL-10, IL-12p70, IL-13, IL17A and tumor necrosis factor alpha (TNF- α). Data were collected using the ProcartaPlex Rat Th Complete Panel 14plexdetection kit (catalog number EPX140-30120–901) following the manufacturer's instructions.

2.15. Newborn astrocyte treatments

After cells reached the confluence, 0.25 mM dibutyryl-cAMP was added for 3 days to induce GLT-1 expression. Then, astrocytes were treated with serum from CLP/sham rats (10% v/v), PBMC CM from CLP/sham rats (10% v/v) and/or 10 μ M LY294002 (a PI3K inhibitor) for different periods (6 h, 24 h and 72 h).

2.16. Peripheral blood mononuclear cells isolation and culture

Fresh heparinized blood from CLP and sham animals was collected 24 h after surgery. Then, blood was gently added over an equal volume of Ficoll-Histopaque. Tubes were centrifuged for 30 min. at 400 xg at room temperature. Next, the opaque interface containing mononuclear cells was transferred into a conical centrifuge tube. PBMCs were washed (centrifuged at 100 xg for 10 min.) twice with sterile HBSS. PBMCs were plated at a density of 1×10^6 cells/mL in a 24-well plate using RPMI-1640 medium supplemented with 10% FBS and kept for 24 h at 37 $^{\circ}$ C in an incubator with 5% CO $_2$ (Shalova et al., 2015). After incubation, the supernatant was collected to perform astrocyte treatments and multiplex analyses.

2.17. Protein determination

Protein content was measured using bicinchoninic acid method with bovine serum albumin as a standard (Smith et al., 1985).

2.18. Statistical analyses

Data were expressed as mean \pm standard deviation (s.d). Normality was evaluated using histograms and quantile plot. All data were normally distributed and comparisons between sham and CLP groups were carried out using Student's *t* test. P-values < 0.05 were reported as statistically significant. Networks were corrected for multiple comparisons using false discovery rate (FDR) *P* < 0.005. GraphPad Prism 6 was used for statistical analysis.

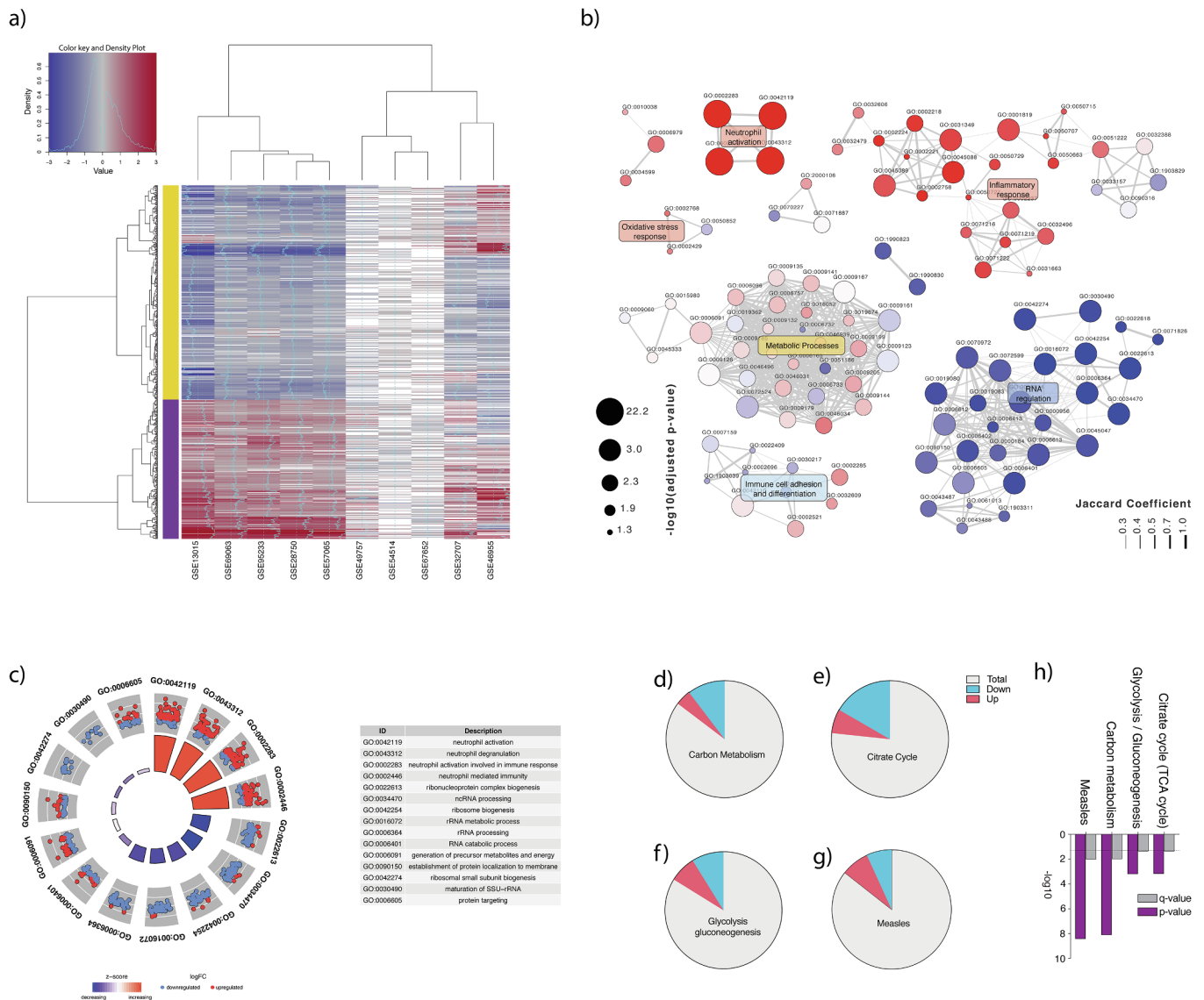


Fig. 1. Transcriptome analyses of blood cells from sepsis patients. The analysis of 10 datasets available on online repositories show differentially expressed genes (DEGs) (a), gene ontology (GO) network (b), the top 10 GO terms up- and downregulated (c) and the enriched KEGG pathways (d-g) and their respective p-value and q-value (h). Only DEGs found in more than 7 datasets were included. In the network, node colors represent the summarized up/downregulation state of the term, while edge widths represent the number of common genes between two terms, summarized in the Jaccard coefficient.

3. Results

3.1. Transcriptome analysis in blood of acute sepsis patients

Transcriptome analysis of peripheral blood cells from 250 healthy subjects and 277 sepsis patients identified a total of 746 differentially expressed genes (DEGs) between groups. Among them, 295 were up-regulated and 451 downregulated (Fig. 1a; Supplementary Table 1; for log Fold change and p-values of each independent dataset, see Supplementary Tables 2 and 3, respectively). Additionally, to verify the biological processes associated with these DEGs we performed an enrichment analysis of gene ontology (GO) biological processes (Supplementary Table 4). Fig. 1b revealed enrichment of DEGs in GO terms related to inflammatory response, energy metabolism, immune cell differentiation and RNA regulation. Top 10 enriched biological processes during sepsis are depicted in Fig. 1c. GO terms associated with immune response are predominant among the upregulated genes, while genes related to RNA processing are dominant in the downregulated DEGs. Finally, to recognize the most affected pathways

related to changes in transcriptome profile, we also performed an enrichment analysis using canonical pathways described in the KEGG pathway database. This revealed a significant enrichment of DEGs in four pathways in septic patients compared to healthy subjects: measles, carbon metabolism, glycolysis/gluconeogenesis and tricarboxylic acid (TCA) cycle (Fig. 1d-h) (for a complete list of up- and downregulated genes in each process, see Supplementary Fig. 2). Interestingly, carbon metabolism, glycolysis/gluconeogenesis and TCA cycle are pathways associated with energy metabolism.

3.2. Acute severe systemic inflammation promotes a shift in astrocyte-mediated cerebral metabolism

Representative micro-PET studies using [¹⁸F]FDG images showed widespread global [¹⁸F]FDG hypometabolism in the CLP group (sham standardized uptake value (SUV) = 2.57 ± 0.38; CLP SUV = 2.07 ± 0.35; Fig. 2a and b). Acute sepsis induced ~ 20% hippocampal [¹⁸F]FDG hypometabolism (Fig. 2c). Fig. 2d depicts hippocampal t-statistical map with peak effect in the posterior area (peak

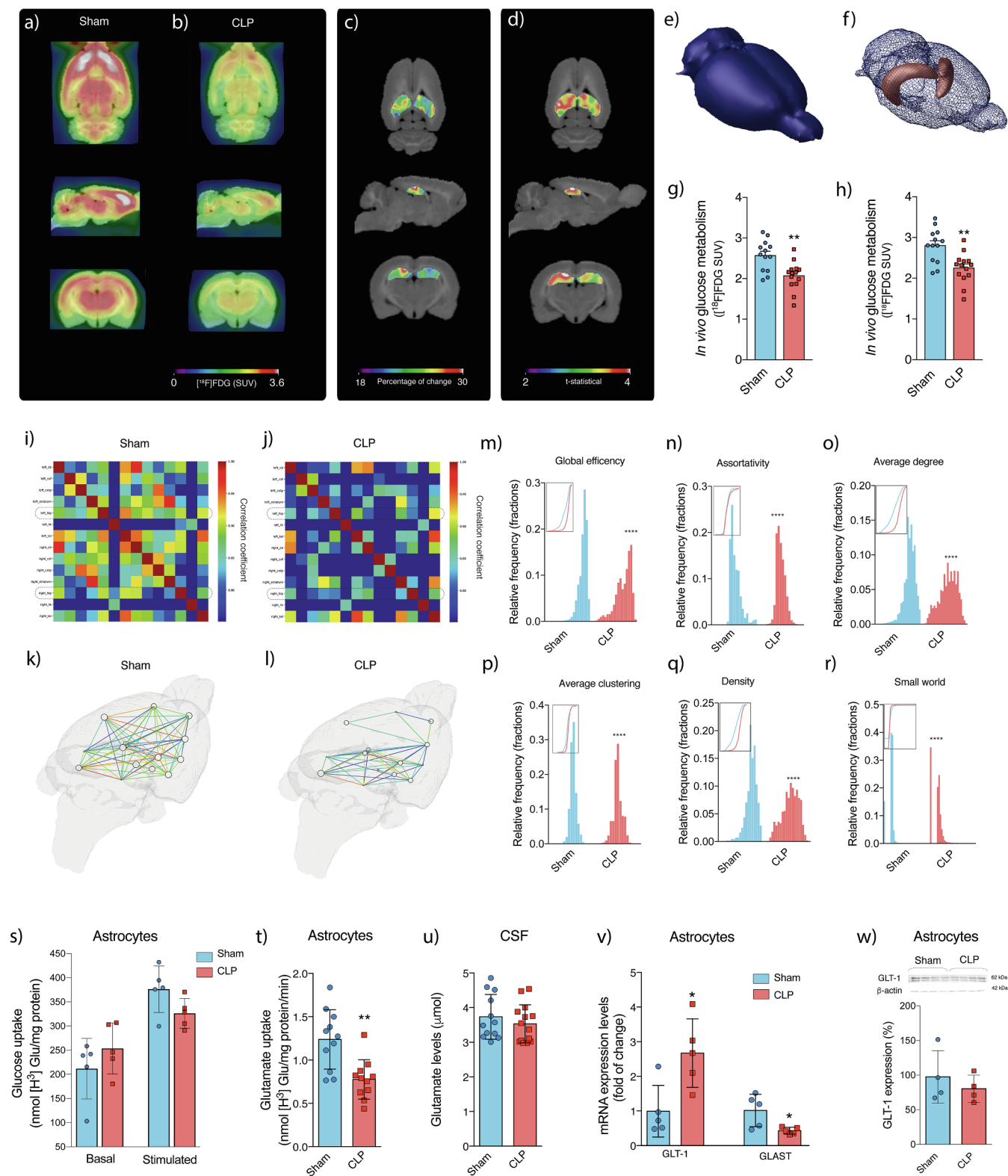


Fig. 2. Astrocytic glucose and glutamate metabolism. Whole-brain [^{18}F]FDG uptake of sham (a) and CLP (b) animals. Percentage of change between sham and CLP (c). T-statistical map overlaid on histological template (d). Brain mask showing VOIs overlaid on histological template (e and f). Whole brain (g) and hippocampal (h) [^{18}F]FDG uptake. Cross-correlation matrices: intersubject cross-correlation maps displaying region-to-region associations in sham (i) and CLP (j) rats. Metabolic networks: 3D brain surfaces displaying large-scale metabolic cross-correlation maps in sham (k) and in CLP (l) animals. Metabolic network graph measures of global efficiency (m), assortativity (n), average degree (o), average clustering (p), density (q) and small world (r). Glucose uptake in astrocytes cultivated from sham and CLP rats (s) Glutamate uptake in astrocytes cultivated from sham and CLP rats (t). Glutamate levels in the CSF (u). GLT-1 and GLAST mRNA levels (v) and immunoccontent in astrocytes cultivated from sham and CLP rats (w). Cumulative frequencies are depicted in the upper left of graph measures (m-r). $n = 5-14$ rats per group. * $P < 0.05$, ** $P < 0.01$, *** $P < 0.001$ (t test). Data are presented as mean values \pm s.d. and individual scatter plots or as correlation values with FDR-corrected ($P < 0.005$) thresholds for brain networks.

$t_{25} = 4.53$; $P = 0.0007$). Whole brain and hippocampal metabolism were chosen as volume of interest (VOIs, Fig. 2e and f). In this way, we identified whole brain ($t_{25} = 3.562$, $P = 0.0015$; Fig. 2g) and hippocampal [^{18}F]FDG hypometabolism ($t_{25} = 3.636$, $P = 0.0013$; Fig. 2h) in animals submitted to CLP. VOIs from all other analyzed brain areas are available in Supplementary Fig. 3. Metabolic networks analyses across previously delineated VOIs were performed to identify brain reorganization patterns during acute sepsis. Sepsis changed multiple connections within the metabolic network, promoting a metabolic hyposynchronicity, especially in hippocampal and cortical areas ($P < 0.005$, FDR corrected, Fig. 2i–l). Graph measures demonstrated a consistent reorganization in the brain metabolic network indexed by lower density ($P < 0.0001$, Fig. 2m), reduced global efficiency ($P = 0.00011$, Fig. 2n), assortativity ($P < 0.0001$, Fig. 2o), small-world ($P < 0.0001$, Fig. 2p), degree ($P < 0.0001$, Fig. 2q) and clustering coefficient ($P < 0.0001$, Fig. 2r) in CLP rats. Aiming to verify a potential coupling between astrocyte glucose and glutamate metabolism during sepsis, astrocyte cultures from CLP and sham rats were performed. Under basal condition, we did not observe any differences in glucose uptake in *ex vivo* astrocytes cultivated from septic rats ($t_8 = 1.148$, $P = 0.284$; Fig. 2s). However, when CLP astrocytes were stimulated with glutamate, we observed a tendency to decrease glucose uptake levels compared to the control ($t_8 = 1.947$, $P = 0.087$; Fig. 2s). Hippocampal astrocytes cultivated from CLP rats presented a significant decrease in glutamate uptake (from 1.22 to 0.78 $\text{nmol}^3[\text{H}]/\text{mg prot}/\text{min}$, $t_{20} = 3.715$, $P = 0.0014$; Fig. 2t). A similar decrease in glutamate uptake was observed in the hippocampal brain slices from rats submitted to surgical sepsis (Supplementary Fig. 4). Complementarily, no changes in glutamate levels in the CSF were verified between groups (Fig. 2u). Astrocytes from CLP animals presented a substantial increase in the mRNA expression levels of GLT-1 (3.4-fold; $t_6 = 4.359$, $P = 0.005$; Fig. 2v). On the other hand, a 2.5-fold decrease in the expression of GLAST was observed in CLP astrocytes when compared to the control group ($t_7 = 2.40$, $P = 0.047$; Fig. 2v). However, no changes in protein levels of GLT-1 were found ($t_6 = 0.801$, $P = 0.454$; Fig. 2w).

3.3. PBMC-released mediators trigger astrocyte reactivity

First, we investigated how the induction of severe systemic inflammation affect astrocytic phenotype in cultivated astrocytes at 24 h post-CLP. We did not observe any major changes in the morphology of astrocytes cultivated from CLP, compared to sham animals (Fig. 3a and b), but CLP astrocytes showed an intense immunostaining for GFAP (Fig. 3c and d). Additionally, astrocytes cultivated from septic rats presented a pronounced diffuse organization of stress fibers, when compared to the parallel and well-organized actin filaments observed in sham astrocytes (Fig. 3e and f). An increase in GFAP protein content was confirmed by western blotting analysis (47%; $P = 0.027$; $t_4 = 3.408$; Fig. 3g). Subsequently, astrocytes cultivated from healthy animals were exposed to the serum collected from CLP animals (serum pro-inflammatory cytokine activation panel is depicted in Fig. 3h; see the absolute values for cytokines in Supplementary Table 5). Interestingly, we observed a dual phase change in astrocytic glutamate uptake after CLP serum exposure. As observed in Fig. 3i, 6 h of septic serum treatment promoted a prominent increase in glutamate uptake (25%, $t_4 = 4.666$, $P = 0.0096$). At the 24 h time-point no changes between astrocytes treated with septic or sham serum were verified ($t_4 = 0.2972$, $P = 0.781$), while a significant decrease in glutamate uptake levels was observed after 72 h of exposure to serum from septic animals compared to sham (31%, $t_4 = 3.080$, $P = 0.036$). Consistently, glucose uptake decreased in astrocytes exposed to 72 h of serum from septic animals (18%, $t_5 = 2.926$, $P = 0.032$; Fig. 3j), mimicking our *in vivo* data. We further analyzed the involvement of PBMC mediators in the activation and shift of astrocyte functions. Conditioned medium collected from PBMCs (PBMC CM), previously isolated from septic or sham animals, was used to treat astrocytes. Cytokine analysis of PBMC

CM pool from septic rats revealed an increase in TNF- α (42%) and IL-10 (15%) and a decrease in G-CSF levels (from 10.02 $\text{pg}/\mu\text{l}$ to undetectable) compared to sham (Fig. 3k). In this way, 72 h of sepsis-activated PBMC CM exposure induced astrocyte reactivity, evidenced by a 2.3-fold increase in the GFAP protein levels (Fig. 3l). Also, a significant decrease in glutamate uptake levels was observed in astrocytes treated with PBMC CM from septic animals ($t_7 = 4.178$, $P = 0.0041$; Fig. 3m), despite no changes in GLT-1 protein expression ($t_6 = 0.827$, $P = 0.004$; Fig. 3n). Additionally, astrocytes exposed to sepsis PBMC CM also showed a prominent decrease in glucose uptake ($t_6 = 4.540$, $P = 0.0039$; Fig. 3o). Corroborating the observations after serum exposure, 24 h of sepsis PBMC CM treatment did not significantly change either glutamate or glucose uptake levels compared to the control conditions (Supplementary Fig. 5). Of note, no significant changes were verified in cell viability after serum or PBMC CM treatments at the time point evaluated in this study (Supplementary Fig. 6). In an attempt to understand the mechanism involved in the astrocytic energetic failure promoted by PBMC mediators, we looked for a potential target among the DEGs found in our transcriptomic analysis. In this sense, we observed a downregulation in two PI3K subunit genes (PIK3C2B and PIK3CD; Supplementary Table 1) along with an upregulation of PTEN (Supplementary Table 1), an important PI3K negative regulator, in septic patients. Based on the evident impairment in the PI3K pathway observed in our transcriptomic analysis and the putative role that this route plays in the management of energetic metabolism, including in glycolysis/gluconeogenesis, we decided to investigate this pathway in our animal model. In this regard, we verified a significant decrease in PI3K phosphorylation in astrocyte cultures exposed to PBMC CM from CLP animals (46%, $t_8 = 4.216$, $P = 0.003$; Fig. 3p). The specific inhibition of PI3K pathway by LY294002 (10 μM) presented a detrimental effect in astrocytes treated with PBMC CM from sham animals, while it exacerbated the decrease observed in glutamate uptake in astrocytes treated with CLP PBMC CM (about 30%, Fig. 3q). Interestingly, LY294002 treatment did not significantly affect glucose uptake levels (Fig. 3r).

4. Discussion

In the present report we described a potential link between peripheral factors and central metabolic failure during the acute phase of a systemic and severe inflammatory episode. We first showed, through a data-driven gene transcription analysis, that pathways related to energy metabolism are the main altered features in the blood of patients during the acute phase of sepsis. Then, in a rat model of sepsis we observed widespread brain energetic abnormalities, including glucose hypometabolism, lower glutamate uptake and astrocyte reactivity. Also, we provided, to the best of our knowledge, the first evidence of mediators released by PBMCs directly promoting astrocyte reactivity during sepsis, in a microglia-independent manner. Finally, by inhibiting PI3K signaling we exacerbated astrocyte dysfunctional glutamate uptake in both sham and CLP groups.

Data-driven transcriptome analysis of blood cells indicated multiple changes in energy metabolism pathways as main features among septic patients. More specifically, we found DEGs overrepresented in carbon metabolism, glycolysis/gluconeogenesis and TCA pathways, indicating a clear impairment in glucose metabolism-related genes. Interestingly, GO terms associated with inflammatory processes were enriched in septic patients but this was not observed in inflammatory KEGG pathways. Our findings associating sepsis-activated PBMCs with peripheral energy metabolism dysfunction motivated us to investigate brain energetics. Since astrocytes are the main glucose handlers in the brain, we decided to assess their functionality during acute sepsis.

Interestingly, we found that the energetic crisis observed in the blood of septic patients was also present in the brains of our CLP rat model. More specifically, we identified widespread brain glucose hypometabolism, as indexed by [^{18}F]FDG PET, in CLP rats. In clinical

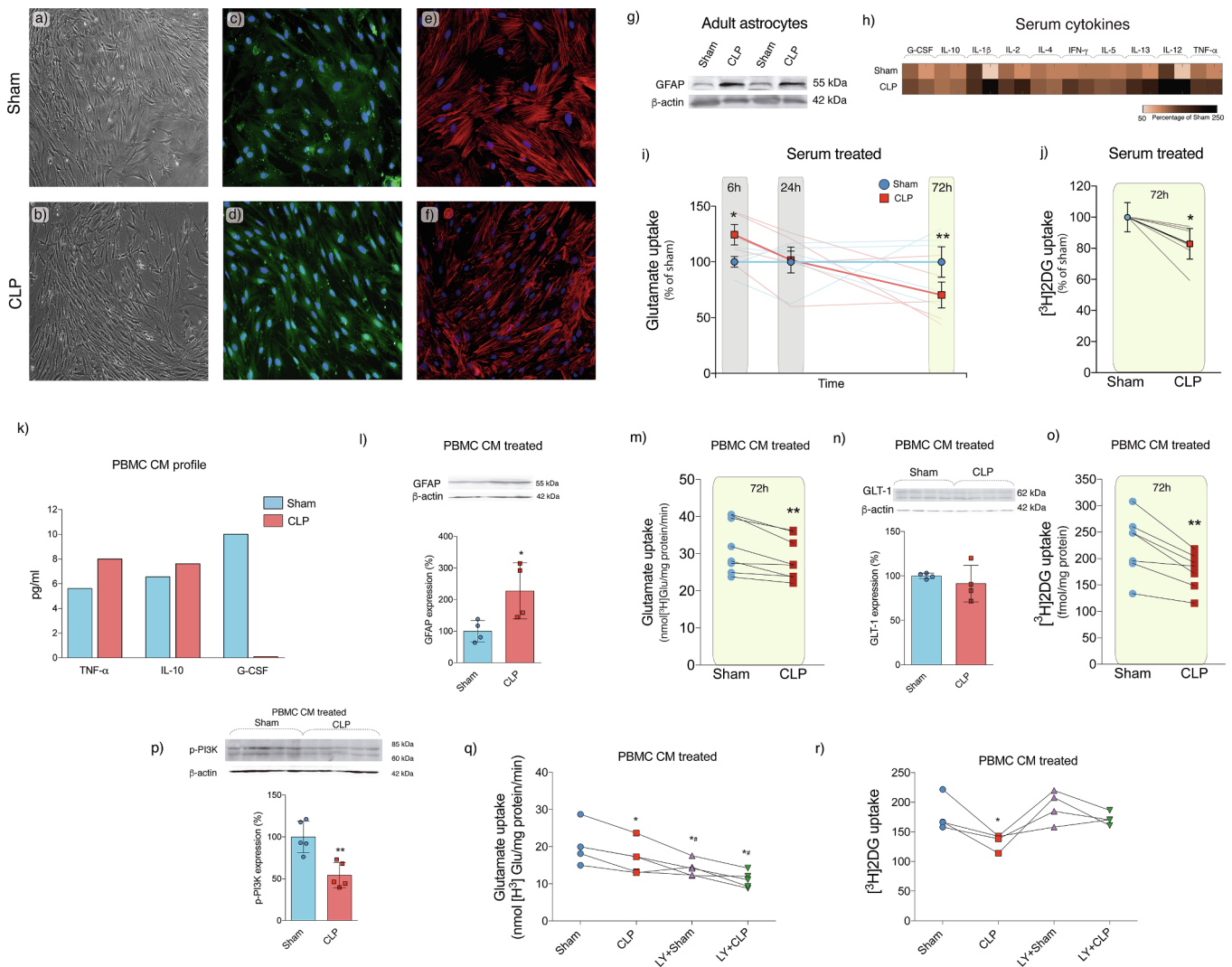


Fig. 3. PBMC released mediators trigger astrocyte activation. Phase contrast (a and b), GFAP immunostaining (c and d) and actin cytoskeleton (e and f) and western blotting for GFAP (g) of astrocytes cultivated from sham and CLP rats. Cytokine profile of serum from sham/CLP rats (h). Glutamate uptake of astrocytes treated with 10% serum from sham/CLP animals for 6 h, 24 h and 72 h (i). Glucose uptake of astrocytes treated with 10% serum from sham/CLP animals for 72 h (j). Cytokine profile of PBMC CM from sham/CLP rats (k). Western blotting for GFAP (l), glutamate (m) and glucose uptake (n) of astrocytes treated with 10% PBMC CM from sham/CLP animals for 72 h. Western blotting for p-PI3K of astrocytes treated with 10% PBMC CM from sham/CLP animals for 72 h (o). Glutamate (q) and glucose uptake (r) by astrocytes pre-treated with 10% PBMC CM from sham/CLP rats and/or 10 μ M LY 294002. $n = 4-6$ per group. * $P < 0.05$, ** $P < 0.01$ (t test). Data are presented as mean values \pm s.d. and individual scatter plots.

settings, [¹⁸F]FDG PET is considered a biomarker of synaptic dysfunction and its values are associated with cognitive impairment (Gardener et al., 2016; Pagani et al., 2015; Weise et al., 2018). Not surprisingly, sepsis has been associated with increased risk for developing dementia (Chou et al., 2017; Cunningham and Hennessy, 2015). Our [¹⁸F]FDG PET regional analysis demonstrated hypometabolism in several brain regions, including the hippocampus. Indeed, other rodent models of sepsis already demonstrated brain [¹⁸F]FDG PET hypometabolism (Semmler et al., 2008; Catarina et al., 2018). In specific, Catarina et al. showed whole brain hypometabolism 12 h after the implantation of a capsule filled with *Escherichia coli* in the peritoneal cavity but did not evaluate regional metabolism (Catarina et al., 2018). Semmler et al. previously demonstrated [¹⁸F]FDG hypometabolism in a lipopolysaccharide (LPS) model of acute sepsis. However, no changes in hippocampal [¹⁸F]FDG PET metabolism were observed in their study (Semmler et al., 2008). Human hippocampi are extremely vulnerable to sepsis, as indexed by hippocampal atrophy in sepsis patients (Semmler et al., 2013). Based on this, one could argue that the CLP model resembles human sepsis with more accuracy than the LPS injection model

(Lee and Huttemann, 2014). In addition, by using refined network analysis, we demonstrated that region-to-region communication in the CLP rat model is largely disrupted. Metabolic network is hyposynchronous in the CLP group and graph measures revealed that brain regions, including the hippocampus, are exchanging information less efficiently.

A recent report demonstrated that glutamate and glucose uptake by astrocytes are coupled, as indexed by [¹⁸F]FDG signal, which suggests that the [¹⁸F]FDG signal also reflects astrocyte metabolism (Zimmer et al., 2017). However, cellular interpretation of [¹⁸F]FDG is still under discussion and we cannot exclude neuronal participation in [¹⁸F]FDG hypometabolism induced by sepsis. For testing this hypothesis, we then evaluated glucose and glutamate uptake *ex vivo* in astrocytes obtained from CLP rats. Interestingly, we did not observe changes in basal glucose uptake between groups. In fact, it seems that the long incubation period required for cultivating mature astrocytes (3–4 weeks) allows them to adapt to environmental conditions, such as high availability of glucose and other nutrients present in the medium. However, we noticed a tendency of lower glucose uptake in CLP astrocytes stimulated

with glutamate, which suggests that these cells still preserved a septic phenotype. Next, we identified that astrocyte glutamate uptake is reduced during acute sepsis but no changes in GLT-1 density, the main glutamate astrocyte transporter (Anderson and Swanson, 2000), were observed. Interestingly, we found increased GLT-1 mRNA expression in CLP astrocytes. Here, we hypothesize that GLT-1 could be either internalized or have its activity reduced, which could explain the lack of changes in transporter density despite reduced glutamate uptake. Also, the 3-fold increase in GLT-1 mRNA suggests that CLP astrocytes are unsuccessfully attempting to replace defective transporters, likely due to the decreased ribosomal protein translation, a process already related to the detrimental effects of sepsis (Hato et al., 2019).

It has been well established that astrocytes are activated during inflammation. Reactive astrocytes overexpress GFAP and release a range of inflammatory cytokines and chemokines (Brahmachari et al., 2006; Gorina et al., 2009). Here we demonstrated PBMC-released factors driving astrocyte reactivity. Serum from CLP animals presented increased levels of pro-inflammatory cytokines, as IL-1 β , IL-12p70, IFN- γ and TNF- α , compared to sham rats. Interestingly, PBMC CM activation was much more subtle (increased TNF- α and IL-10 and decreased G-CSF levels). Indeed, it has been previously demonstrated that even a slight increase in brain TNF- α levels is able to promote a decrease in glutamate transporter activity (Clark and Vissel, 2016), corroborating the deficient glutamate transport observed in our model. In addition, mice lacking TNF- α type 1 receptors had memory preservation after CLP induction (Calsavara et al., 2015). From that, one could argue that astrocyte energy crisis during sepsis seems to be independent of other canonical inflammatory mediators, such as IL-1 β and IFN- γ . However, more studies are required to determine if IL-10 and G-CSF actively play a role in astrocyte activation during sepsis. Of note, we measured only a limited variety of cytokines/chemokines present in the PBMC CM. It is possible that factors not evaluated here are also important for promoting astrocyte reactivity.

The mechanisms involved in the regulation of cerebral energy metabolism during sepsis are poorly understood. The downregulation of PI3K identified in our transcriptome analysis was also observed in astrocytes treated with PBMC CM from CLP rats. Trying to mimic sepsis-induced abnormalities in glutamate and glucose metabolism we conducted a pharmacological inhibition of PI3K in cultured astrocytes. The pharmacological inhibition of PI3K reduced astrocytic glutamate uptake in PBMC CM treated sham and CLP astrocytes. In fact, Zhang et al., also observed that the activation of PI3K signaling increases glutamate uptake by upregulating GLT-1 (Zhang et al., 2013). Additionally, it has been demonstrated that the inhibition of PI3K signaling decreases survival between animals submitted to CLP as well as promotes an early and more severe onset of sepsis (Wrann et al., 2007). The inhibition of PI3K pathway has also been shown to enhance LPS-induced inflammation in different cell types (Guha and Mackman, 2002). Controversially, the inhibition of PI3K did not affect glucose uptake in sham or CLP rats treated with PBMC CM. Based on that, one could argue that PI3K is involved in sepsis-induced glutamate abnormalities but not in mediating glucose hypometabolism, thus inhibiting the signaling at the level of PI3K uncoupled glutamate and glucose metabolism in astrocytes. In this sense, other molecular energy sensors, such as the AMP-activated protein kinase (AMPK), might be acting in parallel with PI3K signaling to regulate glucose uptake (Domise and Vingtdoux, 2016). However, further investigations are needed to completely decode this complex regulation.

Taken together, our results pointed to PBMCs as important triggers of astrocyte reactivity, metabolic and energetic dysfunction during the early stage of sepsis. In addition, we demonstrated that impaired PI3K signaling drives glutamate abnormalities but not glucose hypometabolism during acute sepsis. In summary, this report improves the understanding of the mechanisms by which systemic inflammation impacts brain functionality, indicating potential targets for therapeutic modulation.

5. Data availability

Datasets used in this study can be accessed via NCBI GEO portal (<https://www.ncbi.nlm.nih.gov/geo/>). Further intermediate data and codes generated to implement the MRCMap adaptation are available from the corresponding author upon request.

Funding sources

ERZ receives financial support from CAPES [88881.141186/2017-01], CNPq [460172/2014-0], PRONEX, FAPERGS/CNPq [16/2551-0000475-7], Brazilian National Institute of Science and Technology in Excitotoxicity and Neuroprotection [465671/2014-4], FAPERGS/MS/CNPq/SESRS– PPSUS [30786.434.24734.23112017].

Declaration of Competing Interest

The authors declare there are no conflicts of interest.

Appendix A. Supplementary data

Supplementary data to this article can be found online at <https://doi.org/10.1016/j.bbi.2019.05.041>.

References

- Anderson, C.M., Swanson, R.A., 2000. Astrocyte glutamate transport: review of properties, regulation, and physiological functions. *Glia* 32, 1–14.
- Bellaver, B., Bobermin, L.D., Souza, D.G., Rodrigues, M.D., de Assis, A.M., Wajner, M., Goncalves, C.A., Souza, D.O., Quincozes-Santos, A., 2016a. Signaling mechanisms underlying the glioprotective effects of resveratrol against mitochondrial dysfunction. *Biochim Biophys Acta* 1862, 1827–1838.
- Bellaver, B., Dos Santos, J.P., Leffa, D.T., Bobermin, L.D., Roppa, P.H.A., da Silva Torres, I.L., Goncalves, C.A., Souza, D.O., Quincozes-Santos, A., 2017. Systemic Inflammation as a Driver of Brain Injury: the Astrocyte as an Emerging Player. *Neurobiol. Mol.*
- Bellaver, B., Souza, D.G., Souza, D.O., Quincozes-Santos, A., 2016b. Hippocampal Astrocyte Cultures from Adult and Aged Rats Reproduce Changes in Glial Functionality Observed in the Aging Brain. *Mol Neurobiol.*
- Bergeron, M., Cadorette, J., Tetrault, M.A., Beaudoin, J.F., Leroux, J.D., Fontaine, R., Lecomte, R., 2014. Imaging performance of LabPET APD-based digital PET scanners for pre-clinical research. *Physics in medicine and biology* 59, 661–678.
- Brahmachari, S., Fung, Y.K., Pahan, K., 2006. Induction of glial fibrillary acidic protein expression in astrocytes by nitric oxide. *J Neurosci* 26, 4930–4939.
- Calsavara, A.C., Soriani, F.M., Vieira, L.Q., Costa, P.A., Rachid, M.A., Teixeira, A.L., 2015. TNFR1 absence protects against memory deficit induced by sepsis possibly through over-expression of hippocampal BDNF. *Metabolic brain disease* 30, 669–678.
- Catarina, A.V., Luft, C., Greggio, S., Venturin, G.T., Ferreira, F., Marques, E.P., Rodrigues, L., Wartchow, K., Leite, M.C., Goncalves, C.A., Wyse, A.T.S., Da Costa, J.C., De Oliveira, J.R., Branchini, G., Nunes, F.B., 2018. Fructose-1,6-bisphosphate preserves glucose metabolism integrity and reduces reactive oxygen species in the brain during experimental sepsis. *Brain Res.* 1698, 54–61. <https://doi.org/10.1016/j.brainres.2018.06.024>. Epub 2018 Jun 19. PMID: 29932894.
- Chou, C.H., Lee, J.T., Lin, C.C., Sung, Y.F., Lin, C.C., Muo, C.H., Yang, F.C., Wen, C.P., Wang, I.K., Kao, C.H., Hsu, C.Y., Tseng, C.H., 2017. Sepsis is associated with increased risk for dementia: a population-based longitudinal study. *Oncotarget* 8, 84300–84308.
- Clark, I.A., Vissel, B., 2016. Excess cerebral TNF causing glutamate excitotoxicity rationalizes treatment of neurodegenerative diseases and neurogenic pain by anti-TNF agents. *Journal of neuroinflammation* 13, 236.
- Cunningham, C., Hennessy, E., 2015. Co-morbidity and systemic inflammation as drivers of cognitive decline: new experimental models adopting a broader paradigm in dementia research. *Alzheimer's research & therapy* 7, 33.
- Domise, M., Vingtdoux, V., 2016. AMPK in Neurodegenerative Diseases. *Experientia supplementum* (2012) 107, 153–177.
- Gardener, S.L., Sohrabi, H.R., Shen, K.K., Rainey-Smith, S.R., Weinborn, M., Bates, K.A., Shah, T., Foster, J.K., Lenzo, N., Salvado, O., Laske, C., Laws, S.M., Taddei, K., Verdile, G., Martins, R.N., 2016. Cerebral Glucose Metabolism is Associated with Verbal but not Visual Memory Performance in Community-Dwelling Older Adults. *J Alzheimers Dis* 52, 661–672.
- Godini, R., Fallahi, H., 2018. Network analysis of inflammatory responses to sepsis by neutrophils and peripheral blood mononuclear cells 13, e0201674.
- Gorina, R., Santalucia, T., Petegnief, V., Ejarque-Ortiz, A., Saura, J., Planas, A.M., 2009. Astrocytes are very sensitive to develop innate immune responses to lipid-carried short interfering RNA. *Glia* 57, 93–107.
- Guha, M., Mackman, N., 2002. The phosphatidylinositol 3-kinase-Akt pathway limits lipopolysaccharide activation of signaling pathways and expression of inflammatory mediators in human monocytic cells. *The Journal of biological chemistry* 277,

- 32124–32132.
- Hato, T., Maier, B., Syed, F., Myslinski, J., Zollman, A., Plotkin, Z., Eadon, M.T., Dagher, P.C., 2019. Bacterial sepsis triggers an antiviral response that causes translation shutdown. *The Journal of clinical investigation* 129, 296–309.
- Hornig, S., Therattil, A., Moyon, S., Gordon, A., Kim, K., Argaw, A.T., Hara, Y., Mariani, J.N., Sawai, S., Flodby, P., Crandall, E.D., Borok, Z., Sofroniew, M.V., Chapouly, C., John, G.R., 2017. Astrocytic tight junctions control inflammatory CNS lesion pathogenesis. *J Clin Invest* 127, 3136–3151.
- Iwashyna, T.J., Ely, E.W., Smith, D.M., Langa, K.M., 2010. Long-term cognitive impairment and functional disability among survivors of severe sepsis. *Jama* 304, 1787–1794.
- Kyrkanides, S., Miller, A.W., Miller, J.N., Tallents, R.H., Brouxhon, S.M., Olschowka, M.E., O'Banion, M.K., Olschowka, J.A., 2008. Peripheral blood mononuclear cell infiltration and neuroinflammation in the HexB^{-/-} mouse model of neurodegeneration. *J Neuroimmunol* 203, 50–57.
- Lee, I., Huttemann, M., 2014. Energy crisis: the role of oxidative phosphorylation in acute inflammation and sepsis. *Biochim Biophys Acta* 1842, 1579–1586.
- Livak, K.J., Schmittgen, T.D., 2001. Analysis of relative gene expression data using real-time quantitative PCR and the 2(-Delta Delta C(T)) Method. *Methods (San Diego, Calif.)* 25, 402–408.
- Michels, M., Steckert, A.V., Quevedo, J., Barichello, T., Dal-Pizzol, F., 2015. Mechanisms of long-term cognitive dysfunction of sepsis: from blood-borne leukocytes to glial cells. *Intensive care medicine experimental* 3, 30.
- Murtagg, F., Legendre, P., 2014. Ward's Hierarchical Agglomerative Clustering Method: Which Algorithms Implement Ward's Criterion? *Journal of Classification* 31, 274–295.
- Nortley, R., Attwell, D., 2017. Control of brain energy supply by astrocytes. *Curr Opin Neurobiol* 47, 80–85.
- Pagani, M., De Carli, F., Morbelli, S., Oberg, J., Chincari, A., Frisoni, G.B., Galluzzi, S., Perneczky, R., Drzegza, A., van Berckel, B.N., Ossenkoppele, R., Didic, M., Guedj, E., Brugnolo, A., Picco, A., Arnaldi, D., Ferrara, M., Buschiazzo, A., Sambucetti, G., Nobili, F., 2015. Volume of interest-based [18F]fluorodeoxyglucose PET discriminates MCI converting to Alzheimer's disease from healthy controls. *A European Alzheimer's Disease Consortium (EADC) study. NeuroImage. Clinical* 7, 34–42.
- Pellerin, L., Magistretti, P.J., 2012. Sweet sixteen for ANLS. *J Cereb Blood Flow Metab* 32, 1152–1166.
- Petronilho, F., Perico, S.R., Vuolo, F., Mina, F., Constantino, L., Comim, C.M., Quevedo, J., Souza, D.O., Dal-Pizzol, F., 2012. Protective effects of guanosine against sepsis-induced damage in rat brain and cognitive impairment. *Brain Behav Immun* 26, 904–910.
- Ransohoff, R.M., Schafer, D., Vincent, A., Blachere, N.E., Bar-Or, A., 2015. Neuroinflammation: Ways in Which the Immune System Affects the Brain. *Neurotherapeutics: the journal of the American Society for Experimental Neurotherapeutics* 12, 896–909.
- Richards, M.H., Narasipura, S.D., Kim, S., Seaton, M.S., Lutgen, V., Al-Harhi, L., 2015. Dynamic interaction between astrocytes and infiltrating PBMCs in context of neuroAIDS. *Glia* 63, 441–451.
- Ritchie, M.E., Phipson, B., Wu, D., Hu, Y., Law, C.W., Shi, W., Smyth, G.K., 2015. limma powers differential expression analyses for RNA-sequencing and microarray studies. *Nucleic acids research* 43, e47.
- Rubinov, M., Sporns, O., 2010. Complex network measures of brain connectivity: uses and interpretations. *NeuroImage* 52, 1059–1069.
- Semmler, A., Hermann, S., Mormann, F., Weberpals, M., Paxian, S.A., Okulla, T., Schafers, M., Kummer, M.P., Klockgether, T., Heneka, M.T., 2008. Sepsis causes neuroinflammation and concomitant decrease of cerebral metabolism. *Journal of neuroinflammation* 5, 38.
- Semmler, A., Widmann, C.N., Okulla, T., Urbach, H., Kaiser, M., Widman, G., Mormann, F., Weide, J., Fliessbach, K., Hoefl, A., Jessen, F., Putensen, C., Heneka, M.T., 2013. Persistent cognitive impairment, hippocampal atrophy and EEG changes in sepsis survivors. *Journal of neurology, neurosurgery, and psychiatry* 84, 62–69.
- Shalova, I.N., Lim, J.Y., Chittethath, M., Zinkernagel, A.S., Beasley, F., Hernandez-Jimenez, E., Toledano, V., Cubillos-Zapata, C., Rapisarda, A., Chen, J., Duan, K., Yang, H., Poidinger, M., Melillo, G., Nizet, V., Arnalich, F., Lopez-Collazo, E., Biswas, S.K., 2015. Human monocytes undergo functional re-programming during sepsis mediated by hypoxia-inducible factor-1alpha. *Immunity* 42, 484–498.
- Smith, P.K., Krohn, R.I., Hermanson, G.T., Mallia, A.K., Gartner, F.H., Provenzano, M.D., Fujimoto, E.K., Goeke, N.M., Olson, B.J., Klenk, D.C., 1985. Measurement of protein using bicinchoninic acid. *Analytical biochemistry* 150, 76–85.
- Sofroniew, M.V., 2009. Molecular dissection of reactive astrogliosis and glial scar formation. *Trends Neurosci* 32, 638–647.
- Souza, D.G., Almeida, R.F., Souza, D.O., Zimmer, E.R., 2019. The astrocyte biochemistry. *Seminars in cell. developmental biology*.
- Souza, D.G., Bellaver, B., Bobermin, L.D., Souza, D.O., Quincozes-Santos, A., 2016a. Antagonizing effects of guanosine in glial cells. *Purinergic Signal*.
- Souza, D.G., Bellaver, B., Hansel, G., Arus, B.A., Bellaver, G., Longoni, A., Kolling, J., Wyse, A.T., Souza, D.O., Quincozes-Santos, A., 2016b. Characterization of Amino Acid Profile and Enzymatic Activity in Adult Rat Astrocyte Cultures. *Neurochem Res* 41, 1578–1586.
- Souza, D.G., Bellaver, B., Souza, D.O., Quincozes-Santos, A., 2013. Characterization of adult rat astrocyte cultures. *PLoS One* 8, E60282.
- Tang, B.M., McLean, A.S., Dawes, I.W., Huang, S.J., Lin, R.C., 2009. Gene-expression profiling of peripheral blood mononuclear cells in sepsis. *Critical care medicine* 37, 882–888.
- Weise, C.M., Chen, K., Chen, Y., Kuang, X., Savage, C.R., Reiman, E.M., 2018. Left lateralized cerebral glucose metabolism declines in amyloid-beta positive persons with mild cognitive impairment. *NeuroImage. Clinical* 20, 286–296.
- Wrann, C.D., Tabriz, N.A., Barkhausen, T., Klos, A., van Griensven, M., Pape, H.C., Kendoff, D.O., Guo, R., Ward, P.A., Krettek, C., Riedemann, N.C., 2007. The phosphatidylinositol 3-kinase signaling pathway exerts protective effects during sepsis by controlling C5a-mediated activation of innate immune functions. *J Immunol* 178, 5940–5948.
- Young, G.B., 2010. Sparing brain damage in severe sepsis: a beginning. *Critical care (London, England)* 14, 159.
- Yu, G., Wang, L.G., Han, Y., He, Q.Y., 2012. clusterProfiler: an R package for comparing biological themes among gene clusters. *Omics: a journal of integrative biology* 16, 284–287.
- Zanirati, G., Azevedo, P.N., Venturin, G.T., Greggio, S., Alcara, A.M., Zimmer, E.R., Feltes, P.K., DaCosta, J.C., 2018. Depression comorbidity in epileptic rats is related to brain glucose hypometabolism and hypersynchronicity in the metabolic network architecture. *Epilepsia* 59, 923–934.
- Zhang, X., Shi, M., Bjoras, M., Wang, W., Zhang, G., Han, J., Liu, Z., Zhang, Y., Wang, B., Chen, J., Zhu, Y., Xiong, L., Zhao, G., 2013. Ginsenoside Rd promotes glutamate clearance by up-regulating glial glutamate transporter GLT-1 via PI3K/AKT and ERK1/2 pathways. *Frontiers in pharmacology* 4, 152.
- Ziaja, M., 2013. Septic encephalopathy. *Current neurology and neuroscience reports* 13, 383.
- Zimmer, E.R., Parent, M.J., Souza, D.G., Leuzy, A., Lecrux, C., Kim, H.I., Gauthier, S., Pellerin, L., Hamel, E., Rosa-Neto, P., 2017. [18F]FDG PET signal is driven by astroglial glutamate transport. *Nat. Neurosci.* 20 (3), 393–395. <https://doi.org/10.1038/nn.4492>.
- Cazalis, M.A., Lepape, A., Venet, F., Frager, F., Mouglin, B., Vallin, H., Paye, M., Pachot, A., Monneret, G., 2014. Early and dynamic changes in gene expression in septic shock patients: a genome-wide approach. *Intensive care medicine experimental* 2, 20.
- Dolinay, T., Kim, Y.S., Howrylak, J., Hunninghake, G.M., An, C.H., Fredenburgh, L., Massaro, A.F., Rogers, A., Gazourian, L., Nakahira, K., Haspel, J.A., Landazury, R., Eppanapally, S., Christie, J.D., Meyer, N.J., Ware, L.B., Christiani, D.C., Ryter, S.W., Baron, R.M., Choi, A.M., 2012. Inflammasome-regulated cytokines are critical mediators of acute lung injury. *American journal of respiratory and critical care medicine* 185, 1225–1234.
- Pankla, R., Buddhisa, S., Berry, M., Blankenship, D.M., Bancroft, G.J., Banchereau, J., Lertmemongkolkhai, G., Chaussabel, D., 2009. Genomic transcriptional profiling identifies a candidate blood biomarker signature for the diagnosis of septicemic melioidosis. *Genome biology* 10, R127.
- Parnell, G.P., Tang, B.M., Nalos, M., Armstrong, N.J., Huang, S.J., Booth, D.R., McLean, A.S., 2013. Identifying key regulatory genes in the whole blood of septic patients to monitor underlying immune dysfunctions. *Shock (Augusta, Ga.)* 40, 166–174.
- Sutherland, A., Thomas, M., Brandon, R.A., Brandon, R.B., Lipman, J., Tang, B., McLean, A., Pascoe, R., Price, G., Nguyen, T., Stone, G., Venter, D., 2011. Development and validation of a novel molecular biomarker diagnostic test for the early detection of sepsis. *Critical care (London, England)* 15, R149.
- Venet, F., Schilling, J., Cazalis, M.A., Demaret, J., Poujol, F., Girardot, T., Rouget, C., Pachot, A., Lepape, A., Friggeri, A., Rimmel, T., Monneret, G., Textoris, J., 2017. Modulation of LILRB2 protein and mRNA expressions in septic shock patients and after ex vivo lipopolysaccharide stimulation. *Human immunology* 78, 441–450.
- da Silva, V., Pellegrina, D., Severino, P., Vieira Barbeiro, H., Maziero Andreghetto, F., Tadeu Velasco, I., Possolo de Souza, H., Machado, M.C., Reis, E.M., Pinheiro da Silva, F., 2015. Septic Shock in Advanced Age: Transcriptome Analysis Reveals Altered Molecular Signatures in Neutrophil Granulocytes. *PLoS One* 10, e0128341.